Impact of substrate characteristics on performance of large area plasmonic photoconductive emitters

Nezih T. Yardimci,[1] Rodolfo Salas,[2] Erica M. Krivoy,[2] Hari P. Nair,[2] Seth R. Bank,[2] and Mona Jarrahi[1,*]

[1]*Electrical Engineering Department, University of California Los Angeles, Los Angeles, 90095, USA*
[2]*Electrical and Computer Engineering Department, University of Texas at Austin, Austin, 78758, USA*
[*]*mjarrahi@ucla.edu*

Abstract: We present a comprehensive analysis of terahertz radiation from large area plasmonic photoconductive emitters in relation with characteristics of device substrate. Specifically, we investigate the radiation properties of large area plasmonic photoconductive emitters fabricated on GaAs substrates that exhibit short carrier lifetimes through low-temperature substrate growth and through epitaxially embedded rare-earth arsenide (ErAs and LuAs) nanoparticles in superlattice structures. Our analysis indicates that the utilized substrate composition and growth process for achieving short carrier lifetimes are crucial in determining substrate resistivity, carrier drift velocity, and carrier lifetime, which directly impact optical-to-terahertz conversion efficiency, radiation power, radiation bandwidth, and reliability of large area plasmonic photoconductive emitters.

OCIS codes: (240.6680) Surface plasmons; (300.6495) Spectroscopy, terahertz; (310.6628) Subwavelength structures, nanostructures.

References and links

1. M. Tonouchi, "Cutting-edge terahertz technology," Nat. Photonics **1**(2), 97–105 (2007).
2. D. Graham-Rowe, "Terahertz takes to the stage," Nat. Photonics **1**(2), 75–77 (2007).
3. M. Nagel, M. Forst, and H. Kurz, "THz biosensing devices: fundamentals and technology," J. Phys. Condens. Matter **18**(18), S601–S618 (2006).
4. D. M. Mittleman, R. H. Jacobsen, R. Neelamani, R. G. Baraniuk, and M. C. Nuss, "Gas sensing using terahertz time-domain spectroscopy," J. Appl. Phys. B **67**(3), 379 (1998).
5. K. Kawase, Y. Ogawa, Y. Watanabe, and H. Inoue, "Non-destructive terahertz imaging of illicit drugs using spectral fingerprints," Opt. Express **11**(20), 2549–2554 (2003).
6. D. Grischkowsky, S. Keiding, M. van Exter, and C. Fattinger, "Far-infrared time-domain spectroscopy with terahertz beams of dielectrics and semiconductors," J. Opt. Soc. Am. B **7**(10), 2006 (1990).
7. R. M. Woodward, V. P. Wallace, D. D. Arnone, E. H. Linfield, and M. Pepper, "Terahertz pulsed imaging of skin cancer in the time and frequency domain," J. Biol. Phys. **29**(2/3), 257–259 (2003).
8. D. Van der Weide, J. Murakowski, and F. Keilmann, "Gas-absorption spectroscopy with electronic terahertz techniques," IEEE Trans. Microw. Theory Tech. **48**(4), 740–743 (2000).
9. L. L. Van Zandt and V. K. Saxena, "Millimeter-microwave spectrum of DNA: Six predictions for spectroscopy," Phys. Rev. A **39**(5), 2672–2674 (1989).
10. P. Siegel, "Terahertz technology in biology and medicine," IEEE Trans. Microw. Theory Tech. **52**(10), 2438–2447 (2004).
11. J. F. Federici, B. Schulkin, F. Huang, D. Gary, R. Barat, F. Oliveira, and D. Zimdars, "THz imaging and sensing for security applications-explosives, weapons and drugs," Semicond. Sci. Technol. **20**(7), S266–S280 (2005).
12. N. Nagai, T. Imai, R. Fukasawa, K. Kato, and K. Yamauchi, "Analysis of the intermolecular interaction of nanocomposites by THz spectroscopy," Appl. Phys. Lett. **85**(18), 4010–4012 (2004).
13. M. C. Kemp, P. F. Taday, B. E. Cole, J. A. Cluff, A. J. Fitzgerald, and W. R. Tribe, "Security applications of terahertz technology," Proc. SPIE **5070**, 44–52 (2003).
14. S. Preu, G. H. Dohler, S. Malzer, L. J. Wang, and A. C. Gossard, "Tunable, continuous-wave Terahertz photomixer sources and applications," J. Appl. Phys. **109**(6), 061301 (2011).

#251401 Received 5 Oct 2015; revised 22 Nov 2015; accepted 26 Nov 2015; published 3 Dec 2015

15. C. W. Berry and M. Jarrahi, "Principles of impedance matching in photoconductive antennas," J. Infrared Millim. THz Waves **33**, 1182–1189 (2012).
16. H. Nemec, A. Pashkin, P. Kuzel, M. Khazan, S. Schnull, and I. Wilke, "Carrier dynamics in low-temperature grown GaAs studied by terahertz emission spectroscopy," J. Appl. Phys. **90**(3), 1303 (2001).
17. N. T. Yardimci, S.-H. Yang, C. W. Berry, and M. Jarrahi, "High power terahertz generation using large area plasmonic photoconductive emitters," IEEE Trans. THz Sci. Technol. **5**, 223–229 (2015).
18. M. Jarrahi, "Advanced photoconductive terahertz optoelectronics based on nano-antennas and nano-plasmonic light concentrators," IEEE Trans. THz Sci. Technol. **5**, 391–397 (2015).
19. C. W. Berry, N. Wang, M. R. Hashemi, M. Unlu, and M. Jarrahi, "Significant performance enhancement in photoconductive terahertz optoelectronics by incorporating plasmonic contact electrodes," Nat. Commun. **4**, 1622 (2013).
20. C. W. Berry and M. Jarrahi, "Terahertz generation using plasmonic photoconductive gratings," New J. Phys. **14**(10), 105029 (2012).
21. C. W. Berry, M. R. Hashemi, S. Preu, H. Lu, A. C. Gossard, and M. Jarrahi, "High power terahertz generation using 1550 nm plasmonic photomixers," Appl. Phys. Lett. **105**(1), 011121 (2014).
22. S.-H. Yang, M. R. Hashemi, C. W. Berry, and M. Jarrahi, "7.5% optical-to-terahertz conversion efficiency offered by photoconductive emitters with three-dimensional plasmonic contact electrodes," IEEE Trans. THz Sci. Technol. **4**, 575–581 (2014).
23. C. W. Berry, M. R. Hashemi, and M. Jarrahi, "Generation of high power pulsed terahertz radiation using a plasmonic photoconductive emitter array with logarithmic spiral antennas," Appl. Phys. Lett. **104**(8), 081122 (2014).
24. M. Beck, H. Schäfer, G. Klatt, J. Demsar, S. Winnerl, M. Helm, and T. Dekorsy, "Impulsive terahertz radiation with high electric fields from an amplifier-driven large-area photoconductive antenna," Opt. Express **18**(9), 9251–9257 (2010).
25. A. Dreyhaupt, S. Winnerl, T. Dekorsy, and M. Helm, "High-intensity terahertz radiation from a microstructured large-area photoconductor," Appl. Phys. Lett. **86**(12), 121114 (2005).
26. S. Preu, M. Mittendorff, H. Lu, H. B. Weber, S. Winnerl, and A. C. Gossard, "1550 nm ErAs:In(Al)GaAs large area photoconductive emitters," Appl. Phys. Lett. **101**(10), 101105 (2012).
27. S. Winnerl, "Scalable microstructured photoconductive terahertz emitters," J. Infrared Millim. THz Waves **33**, 431–454 (2012).
28. F. Peter, S. Winnerl, S. Nitsche, A. Dreyhaupt, H. Schneider, and M. Helm, "Coherent terahertz detection with a large-area photoconductive antenna," Appl. Phys. Lett. **91**(8), 081109 (2007).
29. M. Jarrahi, "Terahertz radiation-band engineering through spatial beam-shaping," IEEE Photonics Technol. Lett. **21**(13), 830–832 (2009).
30. M. Jarrahi and T. H. Lee, "High power tunable terahertz generation based on photoconductive antenna arrays," IEEE Microwave Symposium Digest, 391–394 (2008).
31. M. Griebel, J. H. Smet, D. C. Driscoll, J. Kuhl, C. A. Diez, N. Freytag, C. Kadow, A. C. Gossard, and K. Von Klitzing, "Tunable subpicosecond optoelectronic transduction in superlattices of self-assembled ErAs nanoislands," Nat. Mater. **2**(2), 122–126 (2003).
32. H. T. Chen, W. J. Padilla, J. M. O. Zide, S. R. Bank, A. C. Gossard, A. J. Taylor, and R. D. Averitt, "Ultrafast optical switching of terahertz metamaterials fabricated on ErAs/GaAs nanoisland superlattices," Opt. Lett. **32**(12), 1620–1622 (2007).
33. R. P. Prasankumar, A. Scopatz, D. J. Hilton, A. J. Taylor, R. D. Averitt, J. M. Zide, and A. C. Gossard, "Carrier dynamics in self-assembled ErAs nanoislands embedded in GaAs measured by optical-pump terahertz-probe spectroscopy," Appl. Phys. Lett. **86**(20), 201107 (2005).
34. E. M. Krivoy, H. P. Nair, A. M. Crook, S. Rahimi, S. J. Maddox, R. Salas, D. A. Ferrer, V. D. Dasika, D. Akinwande, and S. R. Bank, "Growth and characterization of LuAs films and nanostructures," Appl. Phys. Lett. **101**(14), 141910 (2012).
35. C. W. Berry, N. T. Yardimci, and M. Jarrahi, "Responsivity calibration of pyroelectric terahertz detectors," arXiv:1412.6878v1 (2014).
36. C. Berry, M. R. Hashemi, M. Unlu, and M. Jarrahi, "Design, fabrication, and experimental characterization of plasmonic photoconductive terahertz emitters," J. Vis. Exp. **77**(77), e50517 (2013).

1. Introduction

Photoconductive emitters are widely used in time-domain terahertz imaging and spectroscopy systems for generating pulsed terahertz radiation [1–13]. They are generally comprised of ultrafast photoconductors integrated with terahertz radiating elements on a photo-absorbing semiconductor substrate. When the device is pumped by a femtosecond optical pulse train, photocarriers are generated inside the photo-absorbing semiconductor substrate and drifted by an applied bias electric field to induce a sub-picosecond photocurrent pulse train. The induced photocurrent is then coupled to the terahertz radiating elements to generate pulsed terahertz radiation. While characteristics of the terahertz radiating elements, architecture of the

#251401 Received 5 Oct 2015; revised 22 Nov 2015; accepted 26 Nov 2015; published 3 Dec 2015

photoconductors, and spectral properties of the optical pump beam have direct impact on performance of photoconductive terahertz emitters [14, 15], characteristics of the photo-absorbing semiconductor substrate are also crucial in determining specifications of the generated terahertz radiation. Desired photo-absorbing semiconductor substrates should have high carrier mobility and drift velocity levels to offer high optical-to-terahertz conversion efficiencies. They are also required to have high dark resistivity levels to allow device operation under high bias voltages in order to drift the photocarriers at saturation velocities while maintaining low dark current and thermal dissipation levels. Additionally, short carrier lifetimes are often required to eliminate negative impact of slow photocarriers that do not contribute to efficient terahertz generation but result in device heating and optical-to-terahertz conversion efficiency reduction due to the carrier screening effect and voltage drop across the device active area. Unfortunately, most techniques for developing short carrier lifetime semiconductor substrates introduce high defect density levels inside the semiconductor lattice and, therefore, degrade the carrier mobility and drift velocity of the semiconductor substrate [16]. As a result, choosing optimum photo-absorbing semiconductor substrates for photoconductive terahertz emitters requires an extensive analysis of the tradeoffs between substrate resistivity, carrier lifetime and drift velocity and their impact on terahertz radiation power, radiation bandwidth, thermal dissipation, and device reliability.

In this work, we study the impact of the photo-absorbing semiconductor substrate properties on the performance of large area plasmonic photoconductive emitters operating at an 800 nm wavelength. Large area plasmonic photoconductive emitters have shown a great promise for generating broadband terahertz radiation with record high optical-to-terahertz conversion efficiencies and radiation power levels [17]. The superior properties of large area plasmonic photoconductive emitters are because of using plasmonic contact electrodes that efficiently route a large portion of the photocarriers to the terahertz radiating elements [18–23], which are designed to have dimensions much smaller than the terahertz radiation wavelengths. In addition, use of relatively large device active areas allows handling relatively high optical pump powers without degrading device performance due to the carrier screening effect and thermal breakdown [24–30]. Large area plasmonic photoconductive emitters fabricated on semi-insulating (SI) GaAs substrates offer the highest optical-to-terahertz conversion efficiencies and terahertz radiation power levels at 800 nm optical pump wavelengths [17] because of a higher carrier mobility and drift velocity compared to short carrier lifetime photo-absorbing semiconductor substrates such as low temperature grown (LT) GaAs. However, large area plasmonic photoconductive emitters fabricated on short carrier lifetime substrates such as LT-GaAs offer lower thermal dissipation and better reliability by recombining the slow photocarriers that do not contribute to efficient terahertz generation. Therefore, we study the use of various short carrier lifetime photo-absorbing semiconductor substrates in large area plasmonic photoconductive emitters to gain a deeper understanding of the impact of the substrate properties on terahertz radiation characteristics.

2. Material growth and device fabrication

Materials based on LT-GaAs and superlattice structures of ErAs:GaAs, and LuAs:GaAs are used as the short carrier semiconductor substrates in our study. Recent studies have shown that epitaxially embedded nanoparticles of rare-earth arsenide (RE-As) compounds, such as ErAs and LuAs, can be used as recombination centers, decreasing the carrier lifetime dramatically [31–34]. Moreover, substrate resistivity, mobility, and carrier lifetime can be varied by controlling the RE-As deposition and the superlattice period thickness. ErAs:GaAs and LuAs:GaAs substrates with different RE-As depositions and superlattice periods/thicknesses are grown by solid-source molecular beam epitaxy (MBE) on semi-insulating (100) GaAs substrates. The structures are grown at 530 °C with an As_2/Ga beam equivalent pressure (BEP) ratio of 15 and 3×10^{-6} Torr BEP of As_2, which is held constant throughout the growth of the structures. RE-As nanoparticles are epitaxially incorporated in a

#251401 Received 5 Oct 2015; revised 22 Nov 2015; accepted 26 Nov 2015; published 3 Dec 2015

superlattice structure with depositions of LuAs/ErAs nanoparticles repeated each period. The depositions are reported in terms of equivalent number of LuAs/ErAs monolayers (ML), as determined from reflection high-energy electron-diffraction (RHEED) intensity oscillations and high-resolution X-ray diffraction (HR-XRD) measurements of LuAs/ErAs films. After RE-As deposition, a 50 Å or 100 Å GaAs layer is grown and the structure is repeated 200 or 100 times respectively. For comparison, a LT-GaAs substrate was grown at 250 °C with an As_2/Ga BEP ratio of 19, followed by an annealing process at 600 °C for 10 minutes. The carrier lifetime of the samples are obtained through time-resolved differential optical pump-probe reflection measurements. A list of the materials used in our study together with their carrier lifetimes are shown in Table 1.

Table 1. Carrier lifetime of the grown LT-GaAs, ErAs:GaAs, and LuAs:GaAs compounds

Material	LT-GaAs	ErAs:GaAs (0.5ML/ 100Å) × 100	ErAs:GaAs (0.15ML/ 50Å) × 200	ErAs:GaAs (0.1ML/ 50Å) × 200	LuAs:GaAs (0.5ML/ 100Å) × 100	LuAs:GaAs (0.25ML/ 50Å) × 200	LuAs:GaAs (0.25ML/ 100Å) × 100
Carrier lifetime	0.4 ps	0.93 ps	0.67 ps	0.67 ps	0.8 ps	0.74 ps	0.65 ps

Identical large area plasmonic photoconductive emitters are fabricated on the LT-GaAs, ErAs:GaAs, and LuAs:GaAs substrates and their terahertz radiation performance is analyzed in relation with substrate characteristics. Figure 1(a) shows the schematic diagram of the fabricated large area plasmonic photoconductive emitters. They are designed to have a 0.5 × 0.5 mm^2 active area and 5 μm long plasmonic nanoantenna arrays with 100 nm wide, 50 nm thick, 200 nm spacing Au electrodes and a 350 nm thick Si_3N_4 antireflection coating layer.

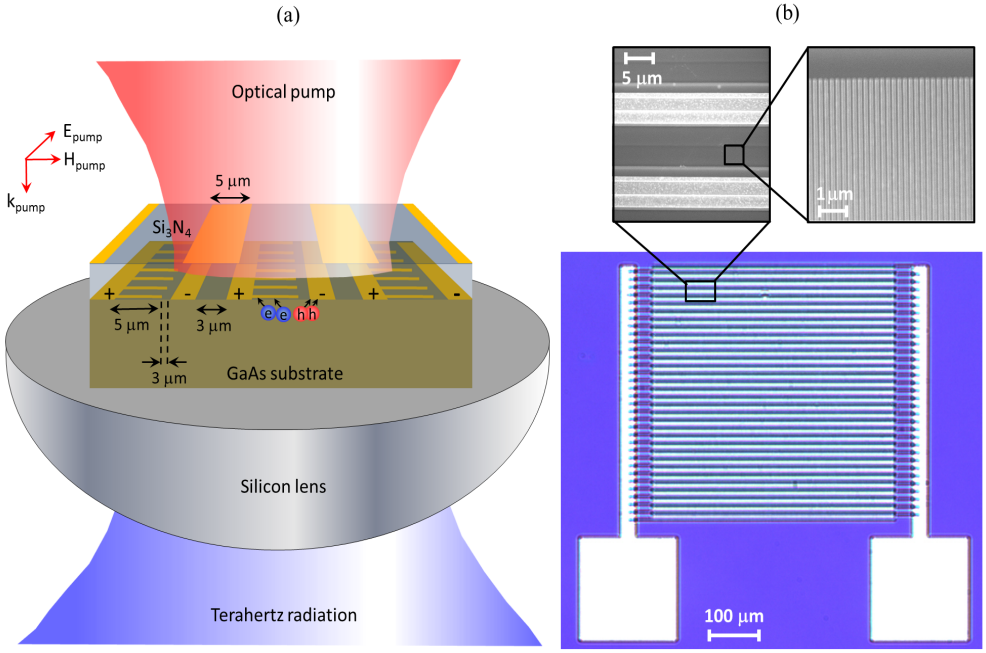

Fig. 1. (a) Schematic diagram and operation concept of the fabricated large area plasmonic photoconductive emitters. (b) Optical microscope and scanning electron microscope (SEM) images of a fabricated large area plasmonic photoconductive emitter prototype.

The nanoantenna geometry is chosen to offer 79% power transmission into the GaAs substrate at 800 nm pump wavelength for a TM-polarized optical pump beam [17]. The plasmonic nanoantennas are connected to anode bias lines of the photoconductive emitter

#251401 Received 5 Oct 2015; revised 22 Nov 2015; accepted 26 Nov 2015; published 3 Dec 2015

within every other gap between the anode and cathode bias lines. The other gaps between the anode and cathode bias lines are shadowed by a second metal layer to block optical pump transmission into the GaAs substrate and prevent destructive interference with the generated terahertz radiation from the nanoantenna arrays.

The optical microscope and scanning electron microscope (SEM) images of a fabricated large area plasmonic photoconductive emitter prototype are shown in Fig. 1(b). The plasmonic nanoantennas are first patterned using electron-beam lithography, followed by 5/45 nm Ti/Au deposition and liftoff. The bias lines are patterned next through optical lithography followed by 50/550 nm Ti/Au deposition and liftoff. The 350 nm Si_3N_4 anti-reflection coating is deposited next using plasma-enhanced chemical vapor deposition (PECVD). The shadow metals are patterned next through optical lithography, followed by 10/90 nm Ti/Au deposition and liftoff. The contact vias are formed next through reactive ion etching of the Si_3N_4 layer. Finally, the device prototypes are mounted on hyper-hemispherical silicon lenses and placed on an optical rotation mount for optical pump polarization adjustments.

3. Experimental characterization and analysis

A mode-locked Ti:sapphire laser at 800 nm with 76 MHz repetition rate and 135 fs pulse width is used as a pump source to characterize the radiation properties of the fabricated large area plasmonic photoconductive emitter prototypes. The measured dark current and photocurrent of the fabricated large area plasmonic photoconductive emitter prototypes are shown in Fig. 2. While the photocurrent levels are directly proportional to the carrier drift velocity and carrier lifetime of the substrates, the dark current levels are directly affected by the resistivity of the substrates, which is a function of the carrier concentration and carrier drift velocity.

A comparison between the dark current and photocurrent of the large area plasmonic photoconductive emitter prototypes fabricated on the LT-GaAs and ErAs:GaAs substrates is shown in Figs. 2(a) and 2(b), respectively. The results indicate a tradeoff between the substrate resistivity and carrier drift velocity for the ErAs:GaAs substrates with different ErAs depositions per superlattice period. The ErAs:GaAs samples with higher ErAs depositions exhibit higher substrate resistivities but offer lower carrier drift velocities, leading to lower induced photocurrent levels. This degrades photoconductive gain and optical-to-terahertz conversion efficiency of the large area plasmonic photoconductive emitters fabricated on the ErAs:GaAs substrates with higher ErAs depositions. On the other hand, the low resistivity nature of the ErAs:GaAs substrates with lower ErAs depositions degrades device reliability and lifetime due to thermal breakdown caused by large dark current levels. Compared with the ErAs:GaAs substrates, the LT-GaAs substrate offers the highest substrate resistivity. Although the induced dark currents in the LT-GaAs sample are much smaller than the induced dark currents in the ErAs:GaAs samples, the induced photocurrent levels in the LT-GaAs sample are in the same order as those of the ErAs:GaAs (0.5ML/100Å) × 100 sample. Considering the carrier lifetime values of the LT-GaAs and ErAs:GaAs substrates, the measured photocurrent levels shown in Fig. 2(b) indicate that the carrier drift velocities in the LT-GaAs substrate are smaller but comparable with the ErAs:GaAs (0.15ML/50Å) × 200 and ErAs:GaAs (0.1ML/50Å) × 200 substrates but larger than the ErAs:GaAs (0.5ML/100Å) × 100 substrate.

A comparison between the dark current and photocurrent of the large area plasmonic photoconductive emitter prototypes fabricated on the LT-GaAs and LuAs:GaAs substrates is shown in Figs. 2(c) and 2(d), respectively. The results indicate similar substrate resistivity levels for the LuAs:GaAs substrates with different LuAs depositions per superlattice period, which are much smaller than the resistivity level of the LT-GaAs substrate. Considering the carrier lifetime values of the LuAs:GaAs substrates, the measured photocurrent levels shown in Fig. 2(d) indicate that the carrier drift velocities in the LuAs:GaAs (0.25ML/100Å) × 100 substrate are much larger than other LuAs:GaAs substrates. This makes the LuAs:GaAs

#251401 Received 5 Oct 2015; revised 22 Nov 2015; accepted 26 Nov 2015; published 3 Dec 2015

(0.25ML/100Å) × 100 substrate a more promising material for large area plasmonic photoconductive emitters, by offering higher photoconductive gain and optical-to-terahertz conversion efficiency levels, accordingly. Considering the carrier lifetime values in the LT-GaAs and LuAs:GaAs substrates, the measured photocurrent levels shown in Fig. 2(d) indicate that the carrier drift velocities in the LT-GaAs substrate are comparable with the LuAs:GaAs (0.5ML/100Å) × 100 and LuAs:GaAs (0.25ML/50Å) × 200 substrates and smaller than the LuAs:GaAs (0.25ML/100Å) × 100 substrate. However, the high resistivity of the LT-GaAs substrate offers better operational reliability due to lower dark currents.

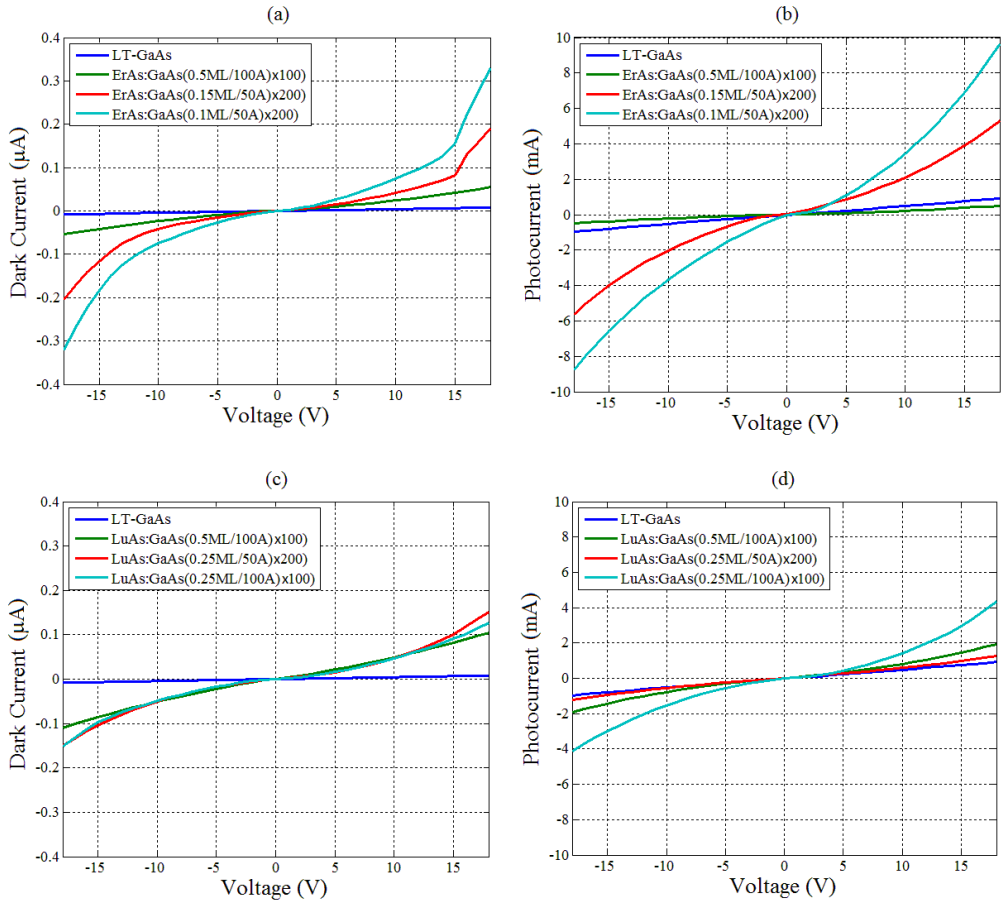

Fig. 2. Measured dark current and photocurrent levels of the large area plasmonic photoconductive emitters fabricated on the LT-GaAs and ErAs:GaAs substrates are shown in (a) and (b), respectively. Measured dark current and photocurrent levels of the large area plasmonic photoconductive emitters fabricated on the LT-GaAs and LuAs:GaAs substrates are shown in (c) and (d), respectively. Photocurrent levels are measured at 800 mW optical pump power.

The radiated terahertz power from the large area plasmonic photoconductive emitter prototypes is measured by using a calibrated pyroelectric detector (Spectrum Detector, Inc. SPIA-65 THz) [35]. A comparison between the radiated terahertz power from the large area plasmonic photoconductive emitter prototypes fabricated on the LT-GaAs and ErAs:GaAs substrates at 800 mW optical pump power is shown in Fig. 3(a). As predicted from the photocurrent measurements, the emitter fabricated on the ErAs:GaAs (0.5ML/100A) × 100 substrate generates the lowest terahertz radiation power levels due to its low carrier drift

#251401 Received 5 Oct 2015; revised 22 Nov 2015; accepted 26 Nov 2015; published 3 Dec 2015

velocities. In addition, the emitter fabricated on the ErAs:GaAs (0.1ML/50A) × 200 substrate generates the highest terahertz radiation power levels due to its high carrier drift velocities.

A comparison between the radiated terahertz power levels from the large area plasmonic photoconductive emitter prototypes fabricated on the LT-GaAs and LuAs:GaAs substrates at 800 mW optical pump power is shown in Fig. 3(b). As expected, similar terahertz power levels are generated from the large area plasmonic photoconductive emitters fabricated on the LT-GaAs, LuAs:GaAs (0.5ML/100A) × 100 and LuAs:GaAs (0.25ML/50A) × 200 substrates due to their comparable carrier drift velocities. The emitter prototype fabricated on the LuAs:GaAs (0.25ML/100A) × 100 substrate generates the lowest terahertz radiation power levels at low bias voltages despite its high carrier drift velocities. This is due to the carrier screening effect, which impacts the LuAs:GaAs (0.25ML/100A) × 100 sample more severely due to its higher carrier drift velocity. However, this carrier screening effect is mitigated at higher bias voltages and is demonstrated by the higher terahertz output powers for voltages above 18 V.

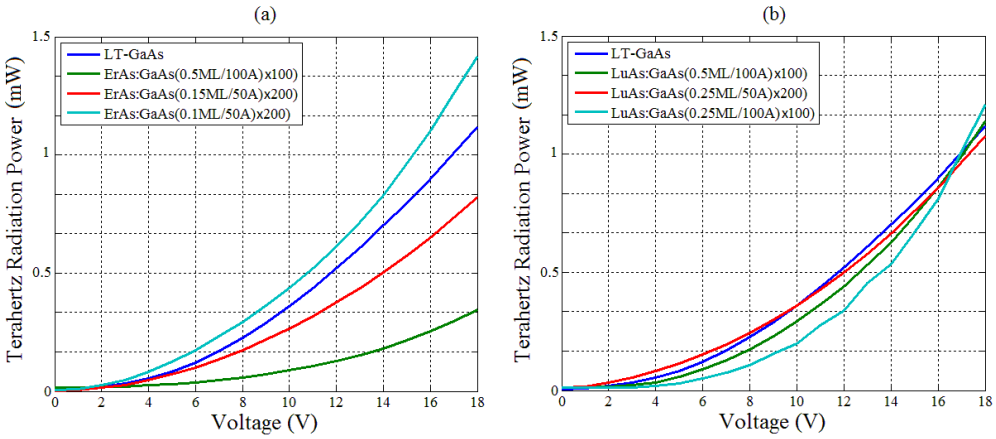

Fig. 3. (a) Measured terahertz power levels at 800 mW optical pump power for the large area plasmonic photoconductive emitters fabricated on the LT-GaAs and ErAs:GaAs substrates. (b) Measured terahertz power levels at 800 mW optical pump power for the large area plasmonic photoconductive emitters fabricated on the LT-GaAs and LuAs:GaAs substrates.

As expected, the device reliability and lifetime of the large area plasmonic photoconductive emitters are directly impacted by their substrate resistivity and photocurrent levels. Thermal breakdown is observed for the large area plasmonic photoconductive emitter prototypes fabricated on the ErAs:GaAs (0.1ML/50A) × 200, ErAs:GaAs (0.15ML/50A) × 200, and LuAs:GaAs (0.25ML/100A) × 100 substrates at 0.9 W, 1 W, and 1.1 W optical pump power and 11.2 mA, 7 mA, and 6.2 mA photocurrent levels at 18 V bias, respectively. No Thermal breakdown is observed for the rest of the emitter prototypes up to 1.2 W optical pump powers.

A time domain terahertz spectroscopy setup with electro-optic detection in a 1 mm ZnTe crystal is used to characterize radiated electric field from the large area plasmonic photoconductive emitter prototypes [36]. In order to prevent thermal breakdown, the emitter prototypes fabricated on the ErAs:GaAs (0.1ML/50A) × 200, ErAs:GaAs (0.15ML/50A) × 200, and LuAs:GaAs (0.25ML/100A) × 100 substrates are pumped at 800 mW optical pump power and the rest of the emitter prototypes are pumped at 1.15 W optical pump power. A bias voltage of 18 V is used for all the measurements. A comparison between the time domain radiated fields from the emitter prototypes fabricated on the LT-GaAs substrate and the ErAs:GaAs and LuAs:GaAs substrates is shown in Figs. 4(a) and 4(b), respectively. As expected, higher terahertz electric fields are radiated from the emitter prototypes fabricated on the substrates with higher carrier drift velocities for the same optical pump powers. As an

#251401 Received 5 Oct 2015; revised 22 Nov 2015; accepted 26 Nov 2015; published 3 Dec 2015

example, at 1.15 W optical pump power, higher terahertz field levels are radiated from the emitter prototypes fabricated on the LT-GaAs substrate compared to the emitter prototypes fabricated on the ErAs:GaAs (0.5ML/100A) × 100 substrate. Similarly, at 800 mW optical pump power, higher terahertz electric field levels are radiated from the emitter prototypes fabricated on the ErAs:GaAs (0.1ML/50A) × 200 substrate compared to the emitter prototypes fabricated on the ErAs:GaAs (0.15ML/50A) × 200 substrate. Additionally, at 1.15 W optical pump power, similar terahertz electric field levels are radiated by the emitter prototypes fabricated on the LT-GaAs, LuAs:GaAs (0.5ML/100A) × 100, and LuAs:GaAs (0.25ML/50A) × 200 substrates.

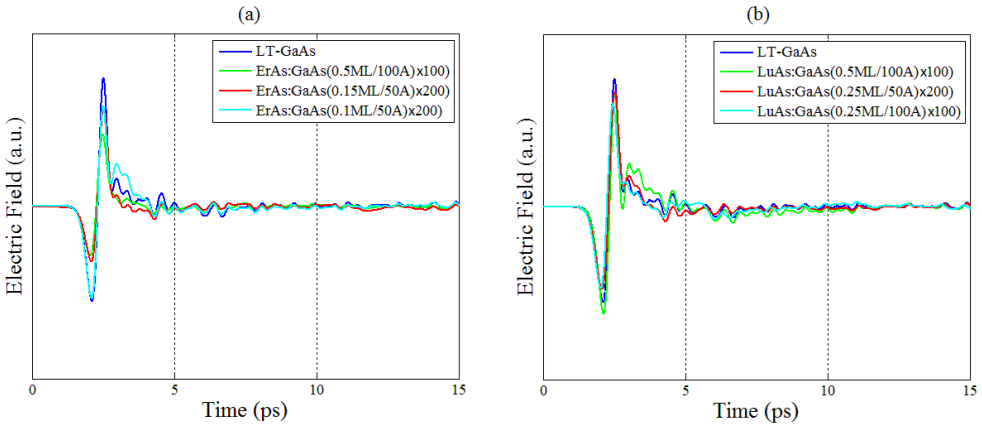

Fig. 4. (a) Radiated electric field in the time domain from the large area plasmonic photoconductive emitters fabricated on the LT-GaAs and ErAs:GaAs substrates. (b) Radiated electric field in the time domain from the large area plasmonic photoconductive emitters fabricated on the LT-GaAs and LuAs:GaAs substrates.

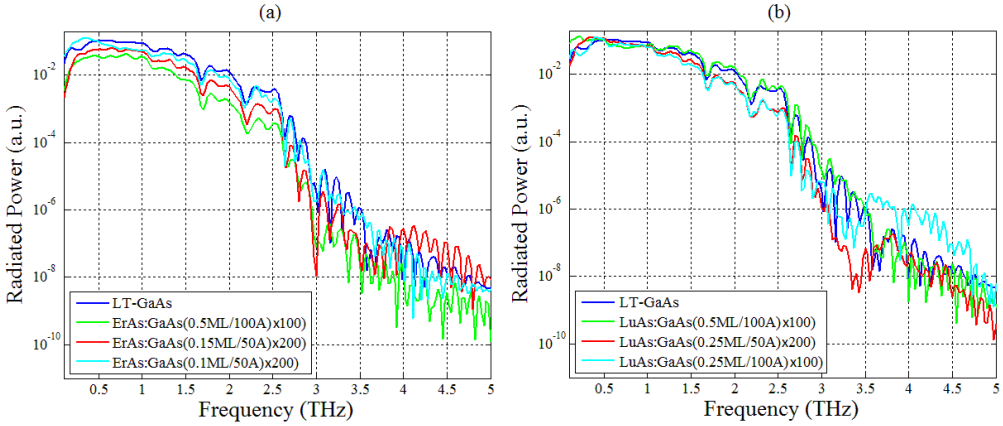

Fig. 5. (a) Radiated spectra from the large area plasmonic photoconductive emitters fabricated on the LT-GaAs and ErAs:GaAs substrates. (b) Radiated spectra from the large area plasmonic photoconductive emitters fabricated on the LT-GaAs and LuAs:GaAs substrates.

The direct impact of the carrier drift velocity on the generated terahertz radiation is also confirmed by comparing the radiation spectra from the emitter prototypes fabricated on the LT-GaAs and the ErAs:GaAs and LuAs:GaAs substrates, shown in Figs. 5(a) and 5(b) respectively. Since the major portion of the generated terahertz radiation from the large area plasmonic photoconductive emitters is due to the ultrafast photocurrent fed to the nanoantenna arrays [17], similar radiation spectral shapes are obtained from the emitter prototypes fabricated on the LT-GaAs, ErAs:GaAs, and LuAs:GaAs substrates. Since the

#251401 Received 5 Oct 2015; revised 22 Nov 2015; accepted 26 Nov 2015; published 3 Dec 2015

magnitude of the photocurrent coupled to the nanoantenna arrays is directly proportional to the carrier drift velocities, higher terahertz radiation power levels are offered by the emitters fabricated on substrates with higher carrier drift velocities utilizing the same optical pump power.

4. Conclusion

In conclusion, we experimentally investigate the impact of short carrier lifetime photo-absorbing semiconductor substrates on the performance of large area plasmonic photoconductive emitters. The terahertz output power and device characteristics are measured under identical conditions for large area plasmonic photoconductive emitters fabricated on LT-GaAs, and superlattice structures of ErAs:GaAs and LuAs:GaAs with different RE-As deposition and superlattice period thicknesses. The results indicate that the utilized substrate composition and growth process for achieving short carrier lifetimes are crucial in determining the substrate resistivity, carrier velocity, and carrier lifetime, which directly impact the characteristics of the generated terahertz radiation. Since the major portion of the generated terahertz radiation from the large area plasmonic photoconductive emitters is due to the ultrafast photocurrent fed to the nanoantenna arrays, higher optical-to-terahertz conversion efficiencies are offered by substrates with higher carrier drift velocities. While ErAs:GaAs and LuAs:GaAs substrates with higher depositions of RE-As degrade carrier drift velocities and, thus, optical-to-terahertz conversion efficiencies, ErAs:GaAs and LuAs:GaAs substrates with lower depositions of RE-As can offer higher carrier drift velocities and optical-to-terahertz conversion efficiencies compared to LT-GaAs. For the same depositions of RE-As, LuAs:GaAs substrates seem to offer higher carrier drift velocities and optical-to-terahertz conversion efficiencies compared to ErAs:GaAs substrates. On the other hand, higher photocurrent levels and lower substrate resistivity levels lead to degraded emitter reliability due to thermal breakdown. Therefore, the large area plasmonic photoconductive emitters fabricated on LT-GaAs offer a more reliable operation at higher optical pump powers. It should be noted that the conclusions of this investigation are not limited to the short carrier lifetime semiconductor substrates used in this study. Similar impact on the performance of large area plasmonic photoconductive emitters is expected for other short carrier lifetime photo-absorbing semiconductor substrates in relation with substrate resistivity, carrier velocity, and carrier lifetime levels.

Acknowledgment

The authors gratefully acknowledge the financial support from Presidential Early Career Award for Scientists and Engineers (# N00014-14-1-0573 & # W911NF-09-1-0434), NSF CAREER Award (# N00014-11-1-0096), ONR Young Investigator Award (# N00014-12-1-0947), and ARO Young Investigator Award (# W911NF-12-1-0253).

#251401 Received 5 Oct 2015; revised 22 Nov 2015; accepted 26 Nov 2015; published 3 Dec 2015